Real-time probing of the electron dynamics of an atom in a strong infrared laser field

Yunpei Deng (邓蕴沛)[1,2,*] and Xinhua Xie (谢新华)[3,†]
[1]*SwissFEL, Paul Scherrer Institut, 5232 Villigen PSI, Switzerland*
[2]*Fritz-Haber-Institut der Max-Planck-Gesellschaft, 14195 Berlin, Germany*
[3]*Photonics Institute, Vienna University of Technology, A-1040 Vienna, Austria*
(Received 13 November 2014; published 22 April 2015)

We present theoretical studies on real-time probing of the electron density evolution of an atom in a strong infrared (IR) laser field with few-cycle near-infrared (NIR) and attosecond extreme-ultraviolet (XUV) pulses. Our results indicate that the electron density near the tunneling barrier is reflected in the additional tunneling ionization yield with a time delayed NIR pulse and the electron density near the nucleus can be probed by the single photoionization yield with a time delayed XUV pulse. It turns out the NIR-probing scheme can be used to study the polarization of the system in an external IR field and the XUV probing can be additionally applied to explore excitation dynamics during and after the IR field interaction.

DOI: 10.1103/PhysRevA.91.043414 PACS number(s): 32.80.Rm, 32.80.Fb, 42.50.Hz

I. INTRODUCTION

Strong field physics, which describes the strong laser field interaction with atoms and molecules, has become a fascinating research direction, especially along the generation of attosecond pulses and their broad applications [1,2]. Strong field phenomena in general involve electron ionization or excitation processes which happen on a very short, femtosecond or attosecond, time scale. There are various probing techniques to time resolve such ultrafast processes. Since a decade ago, the XUV-pump-NIR-probe method has been exploited to measure the Auger decay process and ionization dynamics of noble gases with subfemtosecond resolution [3,4]. Later the attosecond XUV transient absorption spectroscopy has been applied to ultrafast science, e.g., measuring the movement of valence electrons [5], probing the time-dependent molecular dipoles [6], and investigating the autoionization dynamics of atoms [7]. Besides, there are several other probing methods with attosecond temporal resolution but without using attosecond XUV pulses, such as the photoelectron spectroscopy [8–10] and the high-harmonics spectroscopy [11–13].

With the development of ultrafast lasers and the applications of the optical parametric amplification technique, ultrafast strong field physics has been extended from the Ti:Sa based NIR wavelength to the IR regime with wavelengths up to several micrometers [14–18]. IR lasers are versatile sources which have already shown their advantages on the generation of attosecond pulses based on high-harmonic generation [19–22], controlling molecule dissociation [23,24] and studies on filamentation [25]. In strong field physics, the transition from the multiphoton to the tunneling regime for ionization is characterized by the Keldysh parameter [26], which scales quadratically with the laser wavelength. The longer wavelength not only moves the ionization deeper into the tunneling regime, but furthermore allows the control of molecular dissociation at larger internuclear distances. With an IR laser pulse, the increased spacing between successive half-cycles of the laser pulse gives a sufficient time window to capture the dynamics of a subfemtosecond relaxation process, before the identical process is retriggered by the next half-cycle of the laser pulse. Therefore, it provides an ideal tool for field-triggered pump-probe experiments.

In this article, we report theoretical studies on real-time probing of the electron density evolution of an atom in an IR field with few-cycle NIR and attosecond XUV probe pulses. We use ionization yield, a measurable quantity in experiments, as the study object from two-color pump-probe simulations. To make a comparison between NIR probing and XUV probing, we need to understand the ionization mechanisms in both cases. In the case of NIR probing, the tunneling ionization dominates the additional ionization, while in the case of XUV probing, the single-photon ionization dominates the additional ionization because of low pulse intensity and high photon energy. We find the probing quantities follow the electron density near the tunneling barrier for the NIR-probing case and the electron density near the origin of the system for the XUV-probing case, as illustrated in Fig. 1. Because of probing on different quantities, we can get access to the polarization of the electron wave function and the excitation of the system during field interaction of the system with a strong IR field.

II. METHODS

We solve the time-dependent Schrödinger equation with the single-active-electron approximation in a two-dimensional Cartesian coordinate with the pseudospectral method within a spatial box $[-120, 120]$ a.u. in both directions. A step-size-adapted propagator is employed with the Runge-Kutta method to control the numerical errors during the electron wave function evolution in an external field. More details of our simulation methods can be found in Refs. [27,28]. In the simulations, we use a hydrogen-like atomic system which has a ground-state energy of -0.5 a.u. with a screened Coulomb potential $V(x,y) = -1/\sqrt{x^2+y^2+0.64}$. Linearly polarized electric fields along the x coordinate are applied in the simulations. The vector potential A of the laser fields is defined as $A_F(t) = A_{F0}(t-t_F)\sin[\omega_F(t-t_F)+\phi_F]$ with $F =$ XUV, NIR, IR, where ω_F and ϕ_F are the center frequency and the carrier-envelope phase (CEP), respectively. t_F is

*yunpei.deng@psi.ch
†xinhua.xie@tuwien.ac.at

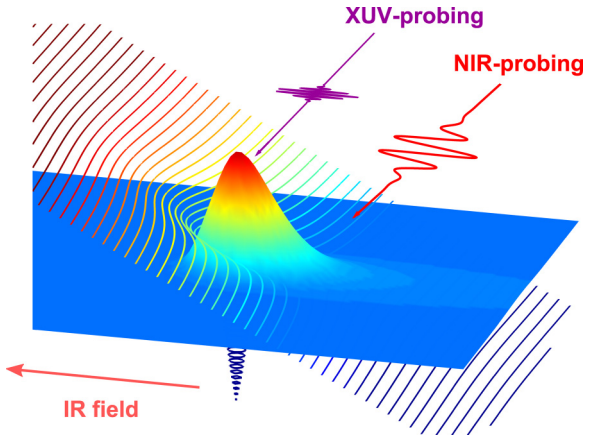

FIG. 1. (Color online) Schematic view of XUV and NIR probing of a strong IR field driven system. The electron density distribution of an IR field distorted ground-state wave function is presented as the color coded surface. The contour lines indicate the tilted Coulomb potential due to the external IR field.

the peak position of the pulse, which is used to control the delays between different pulses. We ensure $A(-\infty) = A(+\infty) = 0$, which excludes any unphysical dc component in the pulses. In the simulations, sine-square envelopes $A_{F0}(t) = (\mathcal{E}_F/\omega_F)\sin^2(\pi t/2\tau_F)$, are used with FWHM τ_F. As shown in Fig. 2(a), pulse durations of XUV, NIR, and IR are chosen as 150 as, 4 fs, and 20 fs, respectively, while their center wavelengths are 20 nm, 800 nm, and 4 μm, respectively. With such pulse durations, both NIR and IR pulses are few-cycle pulses, and their CEPs are critical to the field shapes and important for strong field phenomena [29–31]. For the IR pulse, we choose CEP $= 0.5\pi$ such that the electric field is antisymmetric around the pulse center. The IR pumping pulse has a peak intensity of 1.26×10^{14} W/cm^2. With such intensity, the ionization of the model atom is in the tunneling regime according to the Keldysh parameter $\gamma = 0.27$ [26]. The probing XUV and NIR pulses both have peak intensities of 1×10^{13} W/cm^2. To do the pump-probe simulations, we fix the IR pulse and scan the time delay between the IR pulse and the XUV or NIR pulse by varying t_F of the XUV or NIR pulse.

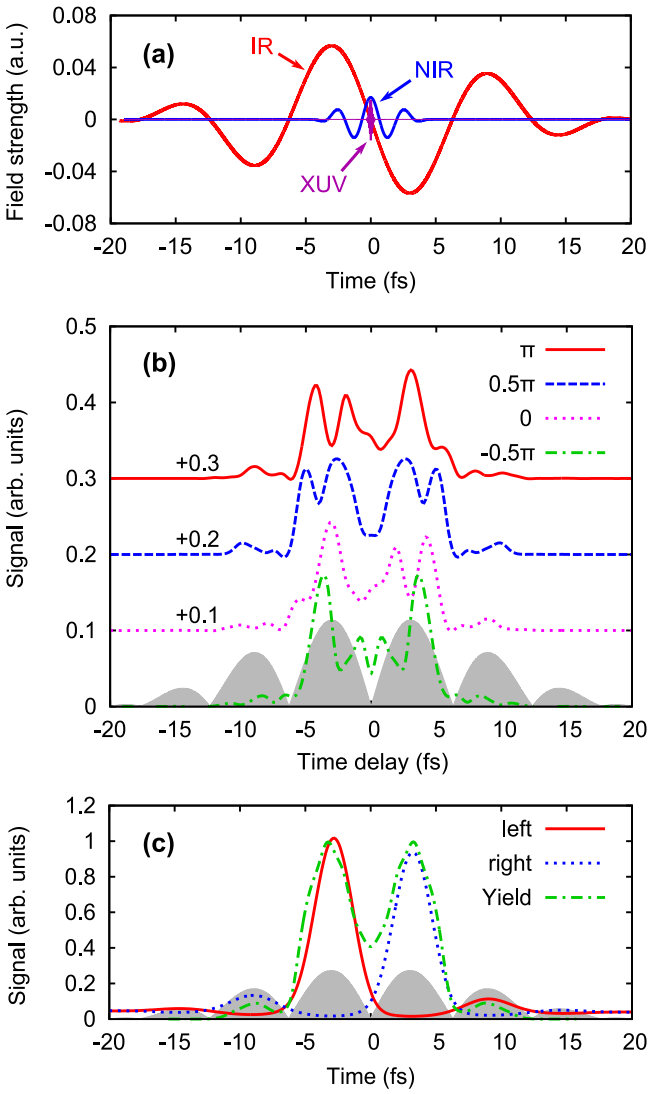

FIG. 2. (Color online) (a) Electric fields of the IR (CEP $= 0.5\pi$), NIR (CEP $= 0$), and XUV pulses used in the simulations. (b) Additional ionization yields as a function of the delay time between NIR and IR pulses for four different CEPs of NIR pulses. Additional amounts of values are added to the signals to have a better comparison. (c) The solid red line and the dashed blue line present normalized electron density at left [at position $(-8,0)$] and right [at position $(8,0)$] sides of the atom over the wave function evolution time in the case of the IR pulse only, respectively. The dash-dotted green line shows the normalized CEP-averaged additional ionization yields as a function of the delay time between NIR and IR pulses. The filled gray lines in (b) and (c) indicate the absolute value of the IR electric field over time.

III. NIR PROBING

First, we present our results on NIR probing. We performed simulations to scan the time delay between the NIR pulse and the IR pulse for four different CEPs $(-0.5\pi, 0, 0.5\pi, \pi)$ of the NIR pulse. To get the ionization yield, we integrate the electron density by projecting the bound states away from the final electron wave function when the laser field is completely off. In Fig. 2(b), we show the additional ionization induced by the combined NIR and IR field, which is defined as $\Delta\eta(\tau) = \eta(\tau)_{\mathrm{NIR+IR}} - \eta_{\mathrm{NIR}} - \eta_{\mathrm{IR}}$, where $\eta(\tau)_{\mathrm{NIR+IR}}$ is the ionization yield with the superimposed field and τ is the time delay. η_{NIR} and η_{IR} are the ionization yields with only the NIR and IR pulse, respectively. It evidently shows that the extra ionization yields have strong modulation over the time delay between the NIR and the IR laser fields for all CEPs. We notice that the change of the yield is mostly positive, which indicates ionization enhancement due to the overlapping of the two pulses. First, we focus on the case of CEP $= 0$ [dotted magenta line in Fig. 2(b)]. The NIR field is a so-called cosine pulse, which has one dominant field peak in the center of the pulse. The modulation of the additional yield follows the intensity of the IR field. It has a maximal peak at a delay time of a quarter optical cycle of the IR pulse before 0, where the IR field has its peak field strength. Intuitively, such modulation depends on the superimposed laser field strength. The field of

the IR field points to the same direction as the NIR peak field at a time delay of a quarter of the optical cycle of the IR pulse before 0, while on the other side of the IR field, the IR field points to the opposite direction. By changing the CEP of the NIR field, the peak strength and the field direction at the time corresponding to the peak field strength changes accordingly. For CEP $= \pi$, the field shape is the same as CEP $= 0$ but the center peak points to the opposite direction, which leads to a maximal peak of additional ionization yield at a time delay of a quarter optical cycle after 0. For the case of CEP $= 0.5\pi$ and CEP $= -0.5\pi$, the NIR fields are antisymmetric which leads to equally strong peaks at positive and negative sides of the time delay. It suggests that the ionization enhancement is caused by the combined wave form of the NIR and IR fields.

To further understand the reason for the enhancement, we calculated the electron density near the nucleus when the atom interacts with an IR-only laser field as shown in Fig. 2(a). In Fig. 2(c), we show the electron density at the left and right sides 8 a.u. away from the nucleus over the evolution time. These positions are below the tunneling barrier when the laser field reaches its peak field strength, which means the electron wave packets at these positions are still bounded. The electron density signal at these two positions follows the electric field of the IR pulse, as shown in Fig. 2(c). On the left side of the nucleus, there are peaks at $t = -3.3$ fs (a quarter of the IR optical cycle before the pulse center) and $t = 9$ fs. On the right side of the nucleus, there are peaks at $t = 3.3$ fs (a quarter of the IR optical cycle after the pulse center) and $t = -9$ fs, which is directly related to the field shape of the IR pulse. It shows that around the peak of the IR field when the potential barrier is bent by the IR field, the wave function will be polarized along the laser polarization direction, such that electron density will be driven to the opposite direction of the laser field, as illustrated in Fig. 1. At this particular time, if additional NIR laser field is applied, ionization will be enhanced when the electric field of the NIR field points to the same direction as that of the IR pulse. To average out the CEP-induced oscillations in the NIR-probing signal, we performed simulations for CEPs from 0 to 2π, and the CEP-averaged additional ionization yield as a function of the time delay between the NIR and IR pulses is presented in Fig. 2(c). It clearly shows that the CEP-averaged additional ionization yields follow the electron density very nicely.

In an intuitive picture, the IR field induces strong polarization of the bound system and part of the electron wave function will be moved to the continuum. The probing NIR field will interact with the polarized bound system and preferentially further tunneling ionizing it from the electron wave function near the tunneling barrier.

IV. XUV PROBING

Now we turn to the case of XUV probing. We investigate how the total XUV photoelectron yields vary during ionization by an IR laser field. We will show that an interpretation of the XUV photoelectron yield in terms of populations of field-free bound states is not possible, but that there is a clear correspondence to the electron density near the nucleus.

The XUV ionization yield is an experimental observable which can be measured with the photoelectron spectroscopy. In the simulations, the XUV ionization yield as a function of time delay τ between the IR pulse and the XUV pulse is calculated as [32,33]

$$Y_{\mathrm{XUV}}(\tau) = |\langle\Psi_{\mathrm{IR}}|\Psi_{\mathrm{IR}}\rangle|^2 - |\langle\Psi_{\mathrm{IR+XUV}}(\tau)|\Psi_{\mathrm{IR+XUV}}(\tau)\rangle|^2, \tag{1}$$

where $\Psi_{\mathrm{IR+XUV}}(\tau)$ is the electron wave function calculated with an XUV pulse, which is delayed by τ with respect to the IR laser pulse, and Ψ_{IR} is the wave function propagated with only the IR laser pulse. The matrix element in Eq. (1) is evaluated at some time $t > \tau$ after the XUV pulse is over. The photon energy of the XUV pulse is 62 eV (much higher than the ionization potential of the system) and the intensity 1×10^{13} W/cm^2, which ensures that the XUV-induced ionization is dominated by the single-photon ionization. During the interaction of the atom with the IR field, the XUV pulse induces extra ionization which is used as the probe signal.

The simulated XUV ionization yields as a function of the time delay between the XUV and IR pulse are presented as green square points in the Fig. 3(a). The XUV ionization yields are normalized to that with the XUV pulse only. The yields oscillate and gradually decrease as scanning through the IR pulse. The oscillation follows the electric field strength of the IR pulse. The yield have local minima at the time delays around the IR field peaks. Intuitively, the XUV ionization yield should be proportional to the electron density in the bound states from which the photoionization happens [4]. To compare this quantity with the XUV ionization yield, we include the population of the ground state and the population of bound states from the $1s$ up to the $4p$ state during the IR-only interaction with the atom in Fig. 3(a) as the solid red line and the dotted blue line, respectively. It is clear that the XUV ionization yield roughly follows the populations of the ground state except that the XUV ionization yield has much stronger modulation. In other words, the XUV ionization yield is not exactly determined by the population in the bound states. We do one more simulation with absorption boundaries such that free electrons will be absorbed by the boundaries at a distance 20 a.u. away from the origin and only bounded electrons stays in the calculation box. The electron density remains in the box then stands for the population of all bounded states, which is presented as the dash-dotted orange line in Fig. 3(a). It has a step-wise structure, and at the end of the laser pulse there is a small amount of discrepancy between the remaining electron density and the population of the ground state. It implies that some populations are left in the excited states after the interaction with the IR laser field. We will further discuss the excitation effect afterwards. So far in the discussion, it has not been clear which quantity the XUV ionization yield represents.

By checking the evolution of the electron density of the system in the IR field, we discover that the electron density near the nucleus matches very nicely with the XUV ionization yield. We define the electron density near the nucleus as

$$N_0(t) = \iint e^{\frac{-1.38(x^2+y^2)}{w^2}} |\Psi_{\mathrm{IR}}(x,y;t)|^2 dx\, dy. \tag{2}$$

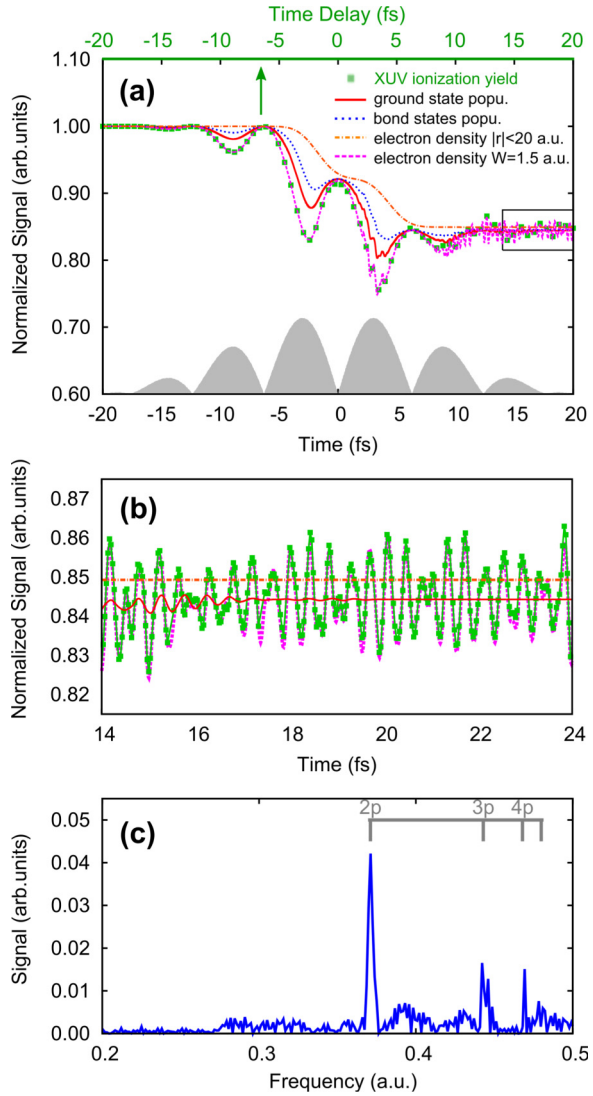

FIG. 3. (Color online) (a) The XUV ionization yields are presented as green square points over the time delay. The population of the ground state and the bound states up to the $4p$ state are shown over time as the solid red line and dotted blue line, respectively. The dashed magenta line and the dash-dotted orange line indicate the electron density near thhe nucleus and the overall electron density (with absorption boundary) of the wave function over time. The gray filled line is the same as those in Fig. 2. (b) A zooming-in of the rectangular region of panel (a) and extension to larger time delay after the IR pulse to present the fast oscillations. (c) The Fourier-transformed spectra of the electron density near the nucleus over time. The gray bar indicates the beating energy between the $2p$, $3p$, and $4p$ states and the $1s$ ground state.

The dashed magenta line in Fig. 3(a) includes $N_0(t)$ using a mask function width $W = 1.5$ a.u. It closely follows the XUV ionization yield when both curves are normalized to 1. Varying the mask function width, the overall shapes of the electron density still follows the XUV ionization yield, but the perfect agreement between them is lost. In the picture in momentum or energy space, the smaller mask function widths select the electrons with higher kinetic energy. Our results also imply that the XUV pulse prefers to remove electrons with high kinetic energy. In a field-free system the electron density at the origin is dominated by the ground-state population, also shown in Fig. 3(a). That quantity has similar characteristics as the XUV-probe signal, but the modulations are less pronounced, which indicates that excited and continuum states influence the XUV-probing process. Note, however, that the effect of the excited state population after the pulse is rather small compared to the modulations of the XUV yield during the pulse. Therefore the participation of excited states during the ionization process can only be of a transient nature, as in adiabatic distortions by the strong field [9].

From the electron density near the nucleus, we observed that there are fast oscillations at the end of the IR pulse. To get insight into this observation, we zoom in this region and extend the time window to 24 fs (note: the IR pulse is over at 20 fs). To show the agreement between the electron density near the nucleus and the XUV yields, we carry out simulations with denser time delay points. Obviously, the perfect agreement preserves. The fast oscillations probed by the XUV probing are similar to the XUV absorption signal measured in experiments [4], which are induced by excitation during the IR field interaction with the atom. Some part of the electron wave function can be excited to np states from the ground $1s$ state through dipole transition. The quantum beating between the ground state and the excited states leads to fast oscillations in the electron density. To further confirm the observed excitation effect, we performed Fourier transformation on the fast oscillating signal in the electron density. As shown in Fig. 3(c), the beating frequencies between the $1s$ ground state and the excited $2p$, $3p$, and $4p$ states are evidently presented. Such results prove that XUV probing can serve as a method to study the excitation dynamics of an atomic or molecular system with attosecond temporal resolution.

V. CONCLUSION

In cases of NIR probing and XUV probing, different quantities are probed due to different ionization mechanisms. Tunneling ionization is more sensitive to the electron density distribution near the tunneling barrier. In other words, the additional ionization yield induced by the NIR pulse reflects the electron density of the polarized system near the tunneling barrier which is some distance away from the nucleus. On the other hand, the XUV pulse probes the electron density of the system near the nucleus, which is not only sensitive to the polarization of the electron wave packet in the laser field but also to the quantum beating between bound states.

In conclusion, we theoretically investigated and compared the NIR probing and XUV probing of the interaction of an atom with a strong IR field. We found that the NIR pulse probes the electron wave function near the tunneling barrier which represents the polarization of the system, while the XUV pulse probes the electron wave function near the nucleus of the atom which can serve for the study of not only polarization but also excitation dynamics from the electron density oscillation due to the quantum beating between different bound states. The underlying physics is different

ionization mechanisms in these two cases. It allows us to acquire electron dynamics information from different spatial regions in the electron wave function of the system by varying the wavelength of the probing pulse. Such knowledge can shed light on ongoing and future probing experiments on atoms and molecules using IR sources to visualize the ultrafast electron motion manifesting IR field induced polarization and excitation.

ACKNOWLEDGMENTS

We thank Dr. Ralph Ernstorfer for fruitful discussions and Christopher Nicholson for improving the writing in the article. This work is financed by the Austrian Science Fund (FWF) (Grant No. P25615-N27) and the European Commission project CRONOS (Grant No. 280879-2). Thanks to the Vienna Scientific Cluster (VSC) for providing computing resources.

[1] A. Scrinzi, M. Y. Ivanov, R. Kienberger, and D. M. Villeneuve, J. Phys. B **39**, R1 (2006).
[2] F. Krausz and M. Ivanov, Rev. Mod. Phys. **81**, 163 (2009).
[3] M. Drescher, M. Hentschel, R. Kienberger, M. Uiberacker, V. Yakovlev, A. Scrinzi, T. Westerwalbesloh, U. Kleineberg, U. Heinzmann, and F. Krausz, Nature **419**, 803 (2002).
[4] M. Uiberacker, T. Uphues, M. Schultze, A. J. Verhoef, V. Yakovlev, M. F. Kling, J. Rauschenberger, N. M. Kabachnik, H. Schröder, M. Lezius *et al.*, Nature **446**, 627 (2007).
[5] E. Goulielmakis, Z.-H. Loh, A. Wirth, R. Santra, N. Rohringer, V. S. Yakovlev, S. Zherebtsov, T. Pfeifer, A. M. Azzeer, M. F. Kling, S. R. Leone, and F. Krausz, Nature **466**, 739 (2010).
[6] C. Neidel, J. Klei, C.-H. Yang, A. Rouzée, M. J. J. Vrakking, K. Klünder, M. Miranda, C. L. Arnold, T. Fordell, A. L'Huillier, M. Gisselbrecht, P. Johnsson, M. P. Dinh, E. Suraud, P.-G. Reinhard, V. Despré, M. A. L. Marques, and F. Lépine, Phys. Rev. Lett. **111**, 033001 (2013).
[7] H. Wang, M. Chini, S. Chen, C.-H. Zhang, Y. Cheng, F. He, Y. Wu, U. Thumm, and Z. Chang, Phys. Rev. Lett. **105**, 143002 (2010).
[8] Y. Huismans, A. Rouzée, A. Gijsbertsen, J. H. Jungmann, A. S. Smolkowska, P. S. W. M. Logman, F. Lépine, C. Cauchy, S. Zamith, T. Marchenko *et al.*, Science **331**, 61 (2011).
[9] X. Xie, S. Roither, D. Kartashov, E. Persson, D. G. Arbó, L. Zhang, S. Gräfe, M. S. Schöffler, J. Burgdörfer, A. Baltuška, and M. Kitzler, Phys. Rev. Lett. **108**, 193004 (2012).
[10] A. E. Boguslavskiy, J. Mikosch, A. Gijsbertsen, M. Spanner, S. Patchkovskii, N. Gador, M. J. J. Vrakking, and A. Stolow, Science **335**, 1336 (2012).
[11] O. Smirnova, Y. Mairesse, S. Patchkovskii, N. Dudovich, D. Villeneuve, P. Corkum, and M. Y. Ivanov, Nature **460**, 972 (2009).
[12] A. Shiner, B. Schmidt, C. Trallero-Herrero, H. Wörner, S. Patchkovskii, P. Corkum, J. Kieffer, F. Légaré, and D. Villeneuve, Nat. Phys. **7**, 464 (2011).
[13] H. Wörner, J. Bertrand, B. Fabre, J. Higuet, H. Ruf, A. Dubrouil, S. Patchkovskii, M. Spanner, Y. Mairesse, V. Blanchet *et al.*, Science **334**, 208 (2011).
[14] G. Andriukaitis, T. Balčiūnas, S. Ališauskas, A. Pugžlys, A. Baltuška, T. Popmintchev, M.-C. Chen, M. M. Murnane, and H. C. Kapteyn, Opt. Lett. **36**, 2755 (2011).
[15] Y. Deng, A. Schwarz, H. Fattahi, M. Ueffing, X. Gu, M. Ossiander, T. Metzger, V. Pervak, H. Ishizuki, T. Taira, T. Kobayashi, G. Marcus, F. Krausz, R. Kienberger, and N. Karpowicz, Opt. Lett. **37**, 4973 (2012).
[16] A. Lanin, A. Fedotov, and A. Zheltikov, JETP Lett. **98**, 369 (2013).
[17] K.-H. Hong, C.-J. Lai, J. P. Siqueira, P. Krogen, J. Moses, C.-L. Chang, G. J. Stein, L. E. Zapata, and F. X. Kärtner, Opt. Lett. **39**, 3145 (2014).
[18] B. W. Mayer, C. R. Phillips, L. Gallmann, M. M. Fejer, and U. Keller, Opt. Lett. **38**, 4265 (2013).
[19] G. Marcus, W. Helml, X. Gu, Y. Deng, R. Hartmann, T. Kobayashi, L. Strueder, R. Kienberger, and F. Krausz, Phys. Rev. Lett. **108**, 023201 (2012).
[20] T. Popmintchev, M.-C. Chen, D. Popmintchev, P. Arpin, S. Brown, S. Ališauskas, G. Andriukaitis, T. Balčiunas, O. D. Mücke, A. Pugzlys *et al.*, Science **336**, 1287 (2012).
[21] C. Gong, J. Jiang, C. Li, L. Song, Z. Zeng, J. Miao, X. Ge, Y. Zheng, R. Li, and Z. Xu, Phys. Rev. A **85**, 033410 (2012).
[22] M.-C. Chen, C. Mancuso, C. Hernández-García, F. Dollar, B. Galloway, D. Popmintchev, P.-C. Huang, B. Walker, L. Plaja, A. A. Jaroń-Becker, A. Becker, M. M. Murnane, H. C. Kapteyn, and T. Popmintchev, Proc. Natl. Acad. Sci. **111**, E2361 (2014).
[23] I. Znakovskaya, P. von den Hoff, G. Marcus, S. Zherebtsov, B. Bergues, X. Gu, Y. Deng, M. J. J. Vrakking, R. Kienberger, F. Krausz, R. de Vivie-Riedle, and M. F. Kling, Phys. Rev. Lett. **108**, 063002 (2012).
[24] Z. Jia, Z. Zeng, R. Li, Z. Xu, and Y. Deng, Phys. Rev. A **89**, 023419 (2014).
[25] D. Kartashov, S. Ališauskas, A. Pugžlys, A. Voronin, A. Zheltikov, M. Petrarca, P. Béjot, J. Kasparian, J.-P. Wolf, and A. Baltuška, Opt. Lett. **37**, 3456 (2012).
[26] L. Keldysh, Sov. Phys. JETP **20**, 1307 (1965).
[27] X. Xie, G. Jordan, M. Wickenhauser, and A. Scrinzi, J. Mod. Opt. **54**, 999 (2007).
[28] X. Xie, M. Wickenhauser, W. Boutu, H. Merdji, P. Salières, and A. Scrinzi, Phys. Rev. A **76**, 023426 (2007).
[29] A. Baltuška, T. Udem, M. Uiberacker, M. Hentschel, E. Goulielmakis, C. Gohle, R. Holzwarth, V. Yakovlev, A. Scrinzi, T. W. Hänsch, and F. Krausz, Nature **421**, 611 (2003).
[30] G. G. Paulus, F. Lindner, H. Walther, A. Baltuska, E. Goulielmakis, M. Lezius, and F. Krausz, Phys. Rev. Lett. **91**, 253004 (2003).
[31] X. Xie, K. Doblhoff-Dier, S. Roither, M. S. Schöffler, D. Kartashov, H. Xu, T. Rathje, G. G. Paulus, A. Baltuška, S. Gräfe, and M. Kitzler, Phys. Rev. Lett. **109**, 243001 (2012).
[32] O. Smirnova, M. Spanner, and M. Y. Ivanov, J. Phys. B **39**, S323 (2006).
[33] O. Smirnova, S. Patchkovskii, and M. Spanner, Phys. Rev. Lett. **98**, 123001 (2007).